1 **The effect of thiamine-coating nanoparticles on their biodistribution and**
2 **fate following oral administration**
3

4 Laura Inchaurraga[1], Ana L Martínez-López[1], Beatrice Cattoz[2], Peter Griffiths[2], Matt
5 Wilcox[3], Jeff Pearson[3], Gemma Quincoces[4], Ivan Peñuelas[4], Nekane Martin-Arbella[1],
6 Juan M. Irache[1,*]
7

8 [1] NANO-VAC Research Group, Department of Chemistry and Pharmaceutical
9 Technology, University of Navarra, Spain
10 [2] Department of Pharmaceutical, Chemical and Environmental Sciences, University of
11 Greenwich, Chatham Maritime, UK.
12 [3] Institute for Cell and Molecular Bioscience, Medical School, Newcastle University,
13 Newcastle Upon Tyne, UK
14 [4] Radiopharmacy Unit, Department of Nuclear Medicine, Clinica Universidad de Navarra,
15 University of Navarra, Spain.
16
17

18 **Corresponding author:**
19 Prof. Juan M. Irache
20 Dep. Chemistry and Pharmaceutical Technology
21 University of Navarra
22 C/ Irunlarrea, 1
23 31008 – Pamplona
24 Spain
25 Phone: +34948425600
26 Fax: +34948425619
27 E-mail: jmirache@unav.es
28
29
30
31

32 **Abstract**
33 Thiamine-coated nanoparticles were prepared by two different preparative methods
34 and evaluated to compare their mucus-penetrating properties and fate *in vivo*. The first
35 method of preparation consisted of surface modification of freshly poly(anhydride)
36 nanoparticles (NP) by simple incubation with thiamine (T-NPA). The second procedure
37 focused on the preparation and characterization of a new polymeric conjugate between
38 the poly(anhydride) backbone and thiamine prior the nanoparticle formation (T-NPB).
39 The resulting nanoparticles displayed comparable sizes (about 200 nm) and slightly
40 negative surface charges. For T-NPA, the amount of thiamine associated to the surface
41 of the nanoparticles was 15 µg/mg. For *in vivo* studies, nanoparticles were labeled with
42 either ^{99m}Tc or Lumogen® Red. T-NPA and T-NPB moved faster from the stomach to the
43 small intestine than naked nanoparticles. Two hours post-administration, for T-NPA and
44 T-NPB, more than 30% of the given dose was found in close contact with the intestinal
45 mucosa, compared with a 13.5% for NP. Interestingly, both types of thiamine-coated
46 nanoparticles showed a greater ability to cross the mucus layer and interact with the
47 surface of the intestinal epithelium than NP, which remained adhered in the mucus
48 layer. Four hours post-administration, around 35% of T-NPA and T-NPB were localized
49 in the ileum of animals. Overall, both preparative processes yielded thiamine decorated
50 carriers with similar physico-chemical and biodistribution properties, increasing the
51 versatility of these nanocarriers as oral delivery systems for a number of biologically
52 active compounds.
53
54 **Keywords:** nanoparticles; thiamine; Vitamin B1; oral delivery; mucus permeating;
55 biodistribution
56
57

2

1. Introduction

The oral route is, in general, perceived by patients as more comfortable and convenient than other routes of drug administration, especially for chronic medication regimens. However, the oral route remains an important challenge that limits the absorption and bioavailability of many biologically active compounds, especially for therapeutic peptides and proteins as well as for drugs suffering from presystemic metabolism. From a biological point of view, the oral delivery of drugs is faced with several main barriers: (i) the acidic pH environment in the stomach, (ii) the enzymatic activity along the gut, (iii) the protective mucus gel layer, (iv) the unstirred water layer adjacent to the epithelium and (v) the surface of absorptive cells, including the glycocalyx. All of these barriers limit the arrival of the unchanged biologically active compound to the portal and/or the systemic circulation (Netsomboon and Bernkop-Schnürch, 2016; Schulz et al., 2015).

In order to overcome these hurdles, different delivery systems have been proposed and are currently under evaluation, including the use of polymer nanoparticles. In principle, some of these delivery systems (acting as nanocarriers) may minimize the effects of extreme pH conditions and digestive enzymes on the stability of the loaded compound, offering significant increases in the oral bioavailability of some drugs (des Rieux et al., 2006; Roger et al., 2010). However, polymer nanoparticles encounter a formidable barrier that significantly limits their arrival at the intestinal epithelium, namely the protective mucus layer lining the epithelium surface of the gut. Thus, most types of these nanoparticles are efficiently trapped in the mucus layer and, then, rapidly eliminated from the mucosa due to the physiological mucus turn-over (Inchaurraga et al., 2015; Suk et al., 2009). In fact, mucus is continuously secreted both to remove pathogens and to lubricate the epithelium as material passes through (Ensign et al., 2012; Pelaseyed et al., 2014).

In order to address this fundamental limitation, an encouraging strategy would be the use of nanoparticles with mucus permeating properties. For this purpose, different strategies have been proposed, including the use of agents to minimize the interaction of nanocarriers with the mucus layer and the application of bio-inspired procedures mimicking key features of microorganisms. Thus, the fluidity of mucus and, hence, the diffusion of nanoparticles through the mucus layer may be increased by either the co-encapsulation of mucolytic agents (e.g., N-acetyl cysteine) (Bourganis et al., 2015) or the binding of proteolytic enzymes (e.g., papain or bromelain) to the surface of nanocarriers in order to cleave locally the glycoprotein substructures of mucus (Pereira de Sousa et al., 2015a). A second interesting approach would be the use of biomimetic strategies, in line with those developed by microorganisms to avoid the protective mucus layer and facilitate its arrival to the intestinal epithelium before invasion and colonization. Within this scenario, virus-mimicking nanoparticles presenting both a hydrophilic shell and a high densely charged surface have been proposed (Pereira de Sousa et al., 2015b). Similarly, the coating of nanoparticles with either bacterial lipopolysaccharide (Gómez et al., 2007) or flagellin from *Salmonella enteritidis* (Salman et al., 2005) was found adequate to specifically target the intestinal epithelium. A further set of strategies would involve the decoration of nanoparticles with hydrophilic ligands in order to minimize the potential hydrophobic interactions of the particles with mucin fibers and other components of the mucus. These "slippery" nanoparticles can be obtained by

using poly(ethylene glycol)s (Iglesias et al., 2017; Laffleur et al., 2014; Zabaleta et al., 2012), mannose (Salman et al., 2006) or thiamine (Salman et al., 2007).

However, one key aspect that sometimes is forgotten during the development and characterization of nanocarriers for mucosal delivery is the combination of the adequate biodistribution properties (including the ability as mucus permeating devices) with a high payload capability. In fact, the encapsulation of a biologically active molecule may significantly modify the physico-chemical properties of empty nanoparticles (Singh and Lillard, 2009) and, hence, negatively affect their ability to reach the epithelium. This fact may limit the potential use of such nanoparticles for delivery purposes. In order to overcome this risk, one possible solution is to develop alternative preparative processes of nanocarriers that are more adapted to the encapsulation of particular groups of drugs, without affecting their biodistribution and fate. In this context, the aim of this work was to prepare thiamine-coated nanoparticles by two different preparative processes and, then, evaluate and compare their mucus permeating properties and behavior *in vivo*.

2. Materials and Methods

2.1. Materials

The copolymer of methyl vinyl ether and maleic anhydride or poly(anhydride) (Gantrez® AN 119; MW: 95.5 kDa when calculated by SEC-MALLS) was supplied by Ashland Inc. (Barcelona, Spain). Thiamine hydrochloride (≥99 %), lactose and calcium chloride were purchased from Sigma-Aldrich (Madrid, Spain). Di-sodium hydrogen phosphate anhydrous and ethanol were provided by Panreac (Barcelona, Spain). Perylene-Red (BASF Lumogen® F Red 305) was from Kremer Pigmente GmbH & Co. (Aichstetten, Germany) and OCT™ Compound Tissue-Tek from Sakura Finetek Europe (Alphen aan Der Rijn, The Netherlands).^{99}Mo-^{99m}Tc generator was purchased from DRYTEC™ (GE Healthcare Bio-science, UK). 4',6-diamidino-2-phenylindole (DAPI) was obtained from Biotium Inc. (Madrid, Spain). Acetone was from (VWR-Prolabo, Linars del Vallès, Spain) and sodium hydroxide and isopropanol from Merck (Madrid, Spain). Deionized water (18.2 MΩ) was prepared by a water purification system (Wasserlab, Pamplona, Spain) and used to prepare all the solutions. The anesthetic isoflurane (Isoflo™) was from Esteve, (Barcelona, Spain). All other chemicals and solvents were of analytical grade.

2.2. Synthesis of the Gantrez® AN-thiamine conjugate (GT)

GT conjugate was obtained by the covalent binding of thiamine to the poly(anhydride) backbone (Figure 1). For this purpose, 5 g Gantrez® AN were dissolved in 200 mL acetone. Then, 125 mg thiamine were added and the mixture was heated at 50°C, under magnetic agitation at 400 rpm, for 3 h. Then, the mixture was filtered through a pleated filter paper and the organic solvent was eliminated under reduced pressure in a Büchi R-144 apparatus (BÜCHI Labortechnik AG, Flawil, Switzerland) until the conjugate was totally dry. By gravimetry, the water content was calculated to be 2.9%.

2.3. Characterization of Gantrez® AN-thiamine conjugate (GT)

The covalent insertion of thiamine in the polymer chain was confirmed by infrared, elemental and titration analysis. The amount of thiamine bound to the poly(anhydride) was estimated by HPLC analysis.

2.3.1 FT-IR analysis

The binding between the poly(anhydride) and thiamine was determined by Fourier transform infrared spectroscopy (FTIR). Spectra were collected in a Nicolet-FTIR Avatar 360 spectrometer (Thermo/Nicolet 360 FT IR E.S.P.; Thermo Fisher Scientific, Waltham, Massachusetts, USA), using a MKII Golden Gate ATR device with resolution of 2 cm^{-1} connected with OMNIC E.S.P. software (Thermo Fisher Scientific, Waltham, Massachusetts, USA). The spectrum obtained was an average of 32 scans.

2.3.2. Elemental analysis

The C, H, O and N contents of the synthesized conjugates were determined in a LECO CHN-900 apparatus (Michigan, USA). For this purpose, 1 mg of each polymer was analyzed by triplicate and the results were expressed as percentage (%w/w).

2.3.3 Titration

The poly(anhydride) and its conjugate were first hydrated and dispersed in water till their total solubilisation. At this moment the aqueous solutions of the polymers were titrated with NaOH 0.2 N in the presence of phenolphthalein, used as indicator. Titration was used to measure the percentage of free carboxylic groups and calculate the degree of substitution (DS) of the resulting conjugate. The decrease of the carboxylic groups in the polymer conjugates in comparison to unmodified Gantrez® AN evidenced the ligand binding.

2.3.4 Thiamine quantification

The amount of thiamine covalently attached to the poly(anhydride) was calculated by a modification of a chromatographic method previously described (Salman et al., 2007). For this purpose, 400 mg Gantrez® AN and 10 mg of thiamine were added to 20 mL acetone. The mixture was heated at 50°C, under magnetic agitation at 400 rpm, for 3 h. The organic solvent was eliminated under reduced pressure in a Büchi R-144 apparatus (BÜCHI Labortechnik AG, Flawil, Switzerland) until the conjugate was totally dry. Once dried, the resulting unpurified conjugate was dissolved in 20 mL of acetone. Then, 40 mL of deionized water were added until the formation of suspension. This suspension was centrifuged for 20 minutes at 41,410 x g and the supernatants were collected for the quantification of thiamine. The analysis was performed in a model 1100 series LC Agilent (Waldbornn, Germany) coupled with a UV diode array detection system. Data were analyzed using the Chem-Station G2171 program. The separation of thiamine was carried out at 40°C on a reversed-phase Zorbax®70Å NH2 column (4.6 × 150 mm; particle size 5 μm) with a Zorbax® original 70Å NH2 guard column (4.6 x 12.5 mm; particle size 5 μm) obtained from Agilent (Waldbornn, Germany). The mobile phase and samples were filtered through a Millipore membrane filter of 0.45 μm. The mobile phase composition was potassium phosphate buffer 50 mM (pH 6) and methanol (80/20, v/v). The flow rate was set to 1 mL/min and the effluent was monitored with UV detection at 254 nm. Standard curves were designed over the range of 10-600 μg/mL (R^2≥0.999) from a thiamine solution in deionized water. Finally, the amount of thiamine associated to the poly(anhydride) backbone was calculated as the difference between the initial amount of thiamine added and the amount of thiamine recovered in the supernatants.

2.4. Preparation of thiamine-coated nanoparticles

Thiamine-coated nanoparticles were prepared from two different experimental procedures.

196 The first one consisted on the incubation of "naked" Gantrez® AN nanoparticles and
197 thiamine following a protocol described previously (Salman et al., 2007) with minor
198 modifications. Briefly, 400 mg Gantrez® AN were dissolved in 20 mL acetone. Then, the
199 nanoparticles were formed by the addition of 40 mL absolute ethanol and 40 mL of
200 distilled water containing 10 mg thiamine. The organic solvents were eliminated under
201 reduced pressure in a BÜCHI R-144 apparatus (BÜCHI Labortechnik AG, Flawil,
202 Switzerland) and the resulting nanoparticles were agitated under magnetic stirring for
203 30 min, at room temperature. Then, the nanoparticles suspensions were purified by
204 centrifugation at 5000 × g for 20 min (SIGMA Lab. centrifuges, Osterode am Harz,
205 Germany) using dialysis tubes Vivaspin® 300,000 MWCO (Sartorius AG, Madrid, Spain).
206 Finally, 800 mg lactose dissolved in 40 mL deionized water was added to the pellet and
207 vortexed for 5 minutes. The resulting suspension of nanoparticles was dried in a Büchi
208 Mini Spray Drier B-290 apparatus (BÜCHI Labortechnik AG, Flawil, Switzerland) under
209 the following experimental conditions: inlet temperature of 90 °C, outlet temperature
210 of 60 °C, spray-flow of 600 L/h, and aspirator at 100% of the maximum capacity. These
211 nanoparticles were named T-NPA.
212 As control, "naked" nanoparticles were prepared in the same way as described
213 previously but in the absence of thiamine. These nanoparticles were identified as NP.
214 The second procedure, using the GT previously synthesized, was based on a controlled
215 desolvation of the conjugate (dissolved in acetone) with water and subsequent
216 stabilization with calcium. For this purpose, 400 mg GT were dissolved in 20 mL acetone
217 and nanoparticles were obtained by the addition of 40 mL purified water containing 1.6
218 mg calcium chloride. Acetone was eliminated under reduced pressure in a BÜCHI R-144
219 apparatus (BÜCHI Labortechnik AG, Flawil, Switzerland) and purified by centrifugation
220 at 5000 × g for 20 min (SIGMA Lab. centrifuges, Osterode am Harz, Germany) using
221 dialysis tubes Vivaspin® 300,000 MWCO (Sartorius AG, Madrid, Spain). Finally, 800 mg
222 lactose dissolved in 40 mL deionized water were added to the pellet and vortexed for 5
223 minutes. The resulting suspension was dried by spray-drying using the same conditions
224 as described above. These nanoparticles based on GT were identified as T-NPB.
225
226 **2.5. Preparation of fluorescently labeled nanoparticles**
227 In all cases, for the fluorescent labeling of nanoparticles, 2 mg Lumogen® F Red 305 were
228 dissolved in the solution of acetone containing the polymer (Gantrez® AN or GT) prior
229 the formation of the nanoparticles as described above. In a similar way, the resulting
230 nanoparticles were purified and dried as aforementioned.
231
232 **2.6. Physico-chemical characterization of nanoparticles**
233 **2.6.1. Size, zeta potential and surface morphology analysis**
234 The mean size and the zeta potential of freeze-dried nanoparticles were determined by
235 photon correlation spectroscopy (PCS) and electrophoretic laser Doppler anemometry,
236 respectively, using a Zetaplus apparatus (Brookhaven Instruments Corporation,
237 Holtsville, USA). In all cases, the size was measured after dispersion of nanoparticles in
238 water whereas the zeta potential was quantified in KCl 0.1 M.
239 The shape and morphology of nanoparticles were examined by scanning electron
240 microscopy (SEM). For this purpose, the powder collected from the spray-drier was
241 dispersed in water and centrifuged at 27,000 × g for 20 min. Then, the pellets were
242 mounted on TEM grids, dried and coated with a palladium-gold layer using a Quorum

243 Technologies Q150R S sputter-coater (Ontario, Canada). SEM was performed using a
244 ZEISS model "Ultra Plus" (Oberkochen, Germany) and LEO 435VP (ZEISS, Cambridge,
245 United Kingdom) high resolution scanning electron microscope.

2.6.2. Thiamine quantification

247 Thiamine (vitamin B1) was quantified in the supernatants obtained during the
248 purification step of nanoparticles by the chromatographic method described above. The
249 standard curves were prepared in supernatant of non-loaded nanoparticles (R^2>0.999).
250 For analysis, samples of 1 mL from the supernatants were transferred to auto-sampler
251 vials, capped and placed in the HPLC auto-sampler. Then, 10 μL aliquot was injected onto
252 the HPLC column. Finally, the amount of thiamine associated to the nanoparticles was
253 calculated as the difference between the initial amount of thiamine added and the
254 amount of thiamine recovered in the supernatants by HPLC.

2.7. Quantification of Lumogen® F red 305

257 The amount of Lumogen® F red 305 loaded in the nanoparticles was quantified by UV-
258 Vis spectrometry at wavelength 573 nm (Labsystems iEMS Reader MF, Vantaa, Finland).
259 For this purpose, 10 mg of the formulations were resuspended in 3 mL water and
260 centrifuged at 41,410 x g for 20 min. Pellets were dissolved in 10 mL acetonitrile 75%.
261 These solutions were finally diluted 1:10 in pure acetonitrile before the analysis.
262 Standard curves were designed over the range of 10-35 μg/mL (R^2≥0.990) from a
263 Lumogen® F red 305 solution in acetonitrile 75% and were prepared in supernatant of
264 non-loaded nanoparticles. Prior the use of fluorescently labelled nanoparticles for *in*
265 *vivo* studies, the stability of the marker in the nanoparticles was assessed by incubation
266 in simulated gastric (pH 1.2, 2 h) and intestinal (pH 6.8, 8 h) fluids.

2.8. Mucin purification from porcine mucus

269 Pig small intestines were obtained from a local abattoir immediately after slaughter and
270 transported on ice to the laboratory. Sections of the intestines that did not visibly
271 contain chyme were cut into 15 cm lengths and mucus was removed. To remove the
272 mucus gentle pressure was applied to one end of the length with the fingers and
273 continuously applied unidirectionally to the opposite end. Mucus gel was added to a
274 cocktail of enzyme inhibitors in phosphate buffer, pH 6.8 (Taylor et al., 2004). The mucin
275 was purified following the protocol described by (Taylor et al., 2004), with the addition
276 of a second cesium chloride gradient to further remove cellular debris from the
277 glycoprotein component of mucus. All freeze dried samples were stored at -20 °C until
278 used.

2.9. Pulsed-Gradient Spin-Echo NMR assessment of mucin mobility

281 In order to evaluate the slippery capacities of nanoparticles, the diffusion of intestinal
282 pig mucin in presence of these nanocarriers was evaluated by pulsed-gradient spin-echo
283 NMR (PGSE-NMR). Measurements were performed on a Bruker DMX400 NMR
284 spectrometer operating at 400 MHz (^{1}H) using a stimulated echo sequence (Callaghan,
285 1991). All the experiments were run at 37 °C using the standard heating/cooling system
286 of the spectrometer to an accuracy of ± 0.3 °C.
287 Generally, the proton NMR spectrum - a series of peaks located at characteristic values,
288 the so-called chemical shifts measured in ppm - is recorded from the solution with
289 increasing intensity of the pulsed-gradients. The self-diffusion coefficient, D, is deduced

by fitting the attenuation (decay) of the integral for a chosen peak to Eq. 1 as a function of the characteristics of the gradient pulses,

$$A (\delta, G, \Delta) = A_0 \exp[-kD] \qquad \text{[Equation 1]}$$

where A is the signal intensity and $k = \gamma^2 G^2 \delta^2 (\Delta - \delta/3)$, given γ is the magnetogyric ration, Δ the diffusion time, δ the gradient pulse length, and G is the gradient field strength. The gradient pulses are ramped to their desired value over a ramp time, σ, typically 250 µs.

For complex spectra such as those encountered here where the observed peaks may arise from different components within the system, or there may be a range of diffusing rates, the diffusion data are better analyzed by fitting to this Eq. 1 the entire spectrum using "CORE", a program devised to resolve the various components present in such data (Stilbs et al., 1996). CORE evaluates the experimental data in two levels, yielding not only estimates of the diffusion coefficients for each component in the sample but also their relative intensities enabling a more insightful analysis of complex datasets. For the mucin diffusion coefficient measurement, the nanoparticles were dispersed in deuterated water (0.5%, w/v) as described before (Pereira de Sousa et al., 2015a). Then, the nanoparticles suspensions were added into an intestinal mucin solution (5% w/v) also in deuterated water and left to equilibrate for 24 h. Finally, 0.6 mL was transferred to 5 mm o.d. Wilmad NMR tubes (Sigma–Aldrich, Haverhill, UK).

2.10. Labelling of nanoparticles with ^{99m}Tc

Nanoparticles were labelled with technetium-99m by reduction with stannous chloride as described previously (Areses et al., 2011). Briefly, 1-2 mCi of freshly eluted ^{99m}Tc-pertechnetate was reduced with 0.03 mg/mL stannous chloride and the pH was adjusted to 4 with 0.1N HCl. Then, an amount of dried powder containing 2 mg nanoparticles were dispersed in 1 mL water prior the addition of the reduced ^{99m}Tc. The mixture was vortexed for 30 s and incubated at room temperature for 10 min. The overall procedure was carried out in helium-purged vials. The radiochemical purity was examined by paper chromatography (Whatman 3MM) developed with NaCl 0.9%. The labelling yield was always over 90%.

2.11. Gastro-intestinal transit studies with radio labelled nanoparticles

These studies were carried out in male Wistar rats weighing 250–300 g that had fasted for 12 h with free access to water. All the procedures were performed following a protocol previously approved by the "Ethical and Biosafety Committee for Research on Animals" at the University of Navarra in line with the European legislation on animal experiments. Animals were briefly stunned with 2% isoflurane gas (flow of oxygen of 0.2 L/min) for administration of nanoparticles (above 1 mL) by oral gavage, and then quickly awakened. Each animal received one single dose of radiolabelled nanoparticles (1 mCi; 0.8-1.0 mg of radiolabelled nanoparticles that were completed with up to 10 mg with unlabelled NP). Three hours after administration of NP, animals were anaesthetised with 2% isoflurane gas (flow of oxygen of 0.2 L/min) and placed in prone position on the gammacamera (Symbia T2 Truepoint; Siemens Medical System, Malvern, USA). SPECT-CT images were acquired for 25 min, with the following parameters for SPECT: 128 x 128 matrix, 90 images, 7 images per second and CT: 110 mAs and 130 Kv, 130 images,

336 slice thickness 3 mm Fused images were processed using the Syngo MI Applications
337 TrueD software.
338
339 **2.12. *In vivo* evaluation of the mucus permeating properties of nanoparticles**
340 These studies were carried out using a protocol described previously (Salman et al.,
341 2007) with minor modifications, after approval by the responsible Committee by the
342 University of Navarra (Ethical and Biosafety Committee for Research on Animals).
343 Briefly, male Wistar rats (average weight 225 g; Harlan, Barcelona, Spain) were placed
344 in metabolic cages and fasted overnight but with free access to water. All animals
345 received orally 25 mg of fluorescently labeled nanoparticles dispersed in 1 mL water. At
346 different times, animals were sacrificed. The abdominal cavity was opened in order to
347 remove the stomach and small intestine, which were removed and carefully rinsed with
348 PBS in order to eliminate the fraction of nanoparticles remaining in the lumen. Then,
349 both the stomach and the small intestine were cut into small portions to facilitate their
350 digestion with NaOH 3M for 24 h and the resulting residues were treated with methanol
351 and centrifuged. Finally, aliquots of the supernatants were assayed for Lumogen$^®$ F Red
352 305 content by spectrofluorimetry (TECAN, Grödig, Austria) at λ_{ex} 485 nm and λ_{em} 540
353 nm.
354 Finally, the tissue distribution of nanoparticles in the gastrointestinal mucosa was
355 visualized by fluorescence microscopy. For that purpose, 25 mg of Lumogen$^®$ F Red-
356 labeled nanoparticles were orally administered to rats as described above. Two hours
357 later, animals were sacrificed by cervical dislocation and the guts were removed. Ileum
358 portions of 1 cm were collected, cleaned with PBS, stored in the tissue proceeding
359 medium O.C.T. and frozen at -80°C. Each portion was then cut into 5-μm sections on a
360 cryostat and attached to glass slides. Finally, these samples were fixed with
361 formaldehyde and incubated with DAPI (4',6-diamidino-2-phenylindole) for 15 minutes
362 before the cover assembly. The presence of both fluorescently loaded poly(anhydride)
363 nanoparticles in the intestinal mucosa and the cell nuclei dyed with DAPI were visualized
364 in a fluorescence microscope (Axioimager M1, Zeiss, Oberkochen, Germany) with a
365 coupled camera (Axiocam ICc3, Zeiss, Oberkochen, Germany) and fluorescent source
366 (HBO 100, Zeiss, Oberkochen, Germany). The images were captured with the software
367 ZEN (Zeiss, Oberkochen, Germany).
368
369 **2.13. Statistical analysis**
370 The *in vivo* data were compared using a one way analisys of the variance (ANOVA)
371 followed by a Tukey-Kremer multicomparison test, using the NCSS 11 statistical software
372 (Kaysville, US). The difference was considered as significant when $P < 0.05$ or $p < 0.001$.
373
374 **3. Results**
375 **3.1. Characterization of Gantrez-thiamine conjugates (GT)**
376 The infrared spectroscopy study of the conjugates (Figure 1) showed the formation of a
377 new binding at ~1650 cm^{-1} associated with the stretching of the new amide group v(C=O)
378 originated as a result of the amine group of the thiamine and the anhydride groups of
379 Gantrez $^®$ AN 119. Besides, the GT spectrum showed a weak band at ~1352 cm^{-1}
380 corresponding to C-N vibrations of thiamine residues (Ferrari et al., 2003).
381 Regarding elemental analysis (Table 1), the binding of thiamine to the polymer backbone
382 slightly decreased the percentage of carbon, whereas the hydrogen content increased.

383 On the other hand, the titration of the hydrated polymer and conjugates confirmed a
384 reduction in the amount of free carboxylic groups by the binding of thiamine to Gantrez®
385 AN (Table 1). In fact, under the experimental conditions used here, about 13% of the
386 maleic anhydride groups of Gantrez® AN were used for the covalent binding of thiamine,
387 generating (from each reactant anhydride group) an amide bond with vitamin B1 and
388 one carboxylic acid residue. In other words, the % of substitution would be of 13%. By
389 HPLC, the amount of thiamine associated to the poly(anhydride) backbone was
390 calculated to be 8.7 μg/mg. Finally, with this data, the MW of the conjugate (GT) was
391 96.33 kDa.

3.2. Preparation of thiamine-coated nanoparticles
394 Thiamine coated nanoparticles were prepared following two different preparative
395 processes. The first method consisted on the preparation of Gantrez® AN nanoparticles
396 (NP or "naked" poly(anhydride) nanoparticles) followed by a thiamine coating
397 procedure (T-NPA). The second method consisted on the preparation of nanoparticles
398 from a Gantrez® AN-thiamine conjugate previously synthetized (T-NPB). Table 2 shows
399 the main physico-chemical properties of the resulting nanoparticles. In all cases, the
400 different nanoparticle formulations displayed a mean size of about 210-230 nm and a
401 negative zeta potential. However, the negative surface charge was slightly lower for
402 thiamine coated nanoparticles (T-NPB), but not statistically significative, than for
403 nanoparticles obtained from the GT (T-NPA) and the "naked" nanoparticles (NP).
404 Interestingly, both preparative procedures produced homogeneous batches of
405 nanoparticles (PDI lower than 0.2) and high yields close to 97.5%. For T-NPA, the amount
406 of thiamine associated to the nanoparticles was 15 μg/mg. Finally, the amount of
407 Lumogen® F Red 305 incorporated into the nanoparticles was calculated to be similar for
408 all the formulations tested and close to 0.7 μg/mg (data not shown).
409 Figure 2 shows the morphological analysis of the different nanoparticle formulations.
410 This analysis by SEM confirmed that all batches of nanoparticles consisted of
411 homogeneous populations of spherical particles. NP presented a smoother surface than
412 thiamine-coated nanoparticles and T-NPB. In addition, T-NPA appeared to be slightly
413 rougher than T-NPB.

3.3. *In vitro* evaluation of the mucus penetrating properties of nanoparticles
416 PGSE-NMR is a non-invasive technique that allows determination of the diffusive
417 character of mucin gel and changes in that dynamic property on addition of selected
418 polymer nanoparticles. The diffusion coefficient is measured from the decrease in
419 intensity of the peaks in the NMR spectrum, a rapidly decaying signal corresponds to
420 high mobility quantified in terms of a large diffusion coefficient (Figure 3).
421 In complex systems such as those being examined here, it is quite common for the data
422 to show more than one diffusive rate. These may arise due to the presence of several
423 components that each shows peaks at the same chemical shift (so-called overlapping
424 spectra) or that particular component being present in different physical environments,
425 e.g. gelled or non-gelled materials. Under those circumstances, it is first useful to
426 consider an average diffusion coefficient, being the signal intensity-weighted value of
427 the other discrete values, Table 3, when the different nanoparticle formulations used in
428 this study have been added to the mucin samples. Analysing the ratio of the mean
429 diffusion coefficients i.e. the mucin plus NP value divided by the value from the mucin-

only sample, shows that the mucin diffusion was largely unchanged for the control particle (row "NP"). On the contrary, the ratio of the weighted mucin diffusion coefficients increased a factor of 5-fold when both thiamine decorated nanoparticles were incubated with mucin, addition of the nanoparticles increased the dynamics of the mucin.

Focusing on the detail within the analysis, the entire PGSE-NMR spectra for mucin alone fitted best to two diffusive rates, (Figure 3A), with peaks occurring at similar chemical shifts for both components i.e. the same material. The most straightforward interpretation would be that the gelled fraction of the mucin (sometimes called "firm") corresponds to the slower diffusing component, (D_{slow}= 2.1 E-13 m^2/s), representing 21% of the signal, whereas the faster term - the greater component - is the non-gelled fraction (D_{fast}= 8.3E-12 m^2/s; 79% of the signal). Interestingly, when nanoparticles were added to the mucin sample, a third much slower diffusive rate appeared (Figure 3B), respect to the other two components, indicating modification of the structure of the mucin gel. This modification decreases the mobility of some of the mucin but significantly increases the mobility of another portion. Notwithstanding the emergence of this slow component, the diffusion of the bulk of the mucin increased (Table 3, columns D2 and D3), with the principle component and the average value some 4-5x times higher for thiamine decorated nanoparticles than for the naked poly(anhydride) nanoparticles.

3.4. Biodistribution studies with ^{99m}Tc radiolabelled nanoparticles

Figure 4 shows the comparison of the biodistribution of nanoparticles (after radiolabelling with ^{99m}Tc) when administered by the oral route to laboratory animals. In all cases, 2 hours post-administration, nanoparticles were visualized in the stomach and the small intestine of animals. However, the intensity of the radioactivity in the stomach of animals was higher for NP than for T-NPA and T-NPB. On the contrary, nanoparticles containing thiamine appeared to move faster than NP because the radioactivity was more intense in the small intestine than in the stomach of animals. Interestingly, no activity was observed in the liver or the lungs of the animals.

3.5. Evaluation of the mucus permeating properties of nanoparticles

Figure 5 shows the evaluation of the interaction of nanoparticles with the surface of the stomach mucosa and the small intestine expressed as the adhered fraction of the given dose. In all cases the animals received a dose of 25 mg of nanoparticles dispersed in 1 mL water. Two hours post-administration (Figure 5A), significant differences were found between control nanoparticles (NP), which displayed a significantly higher capability to interact with the stomach mucosa than nanoparticles containing thiamine (p<0.05). Actually, the fraction of the given dose in close contact with the stomach mucosa was almost 3-fold higher than T-NPA and almost 14-fold higher than for T-NPB.

Interestingly, in the small intestine, the capability of NP to interact with the mucosa was significantly lower than for nanoparticles containing thiamine. In fact, both T-NPA and T-NPB presented a strong capability to remain close contact with the surface of the small intestine (mainly in the I2 segment corresponding with the distal jejunum and proximal ileum). Thus, for both types of nanoparticles, more than 30% of the given dose was found in close contact with the surface of the mucosa, compared with a 13.5% in the case of NP.

477   Four hours post-administration (Figure 5B), the remained fraction of NP in close contact
478   with the gut mucosa was very low. Only a small amount was quantified in the distal
479   region of the ileum and caecum. On the contrary, for T-NPA and T-NPB, about 35% of
480   the given dose was mainly localized in the ileum of animals (segments I2 and I3). Overall,
481   no significant differences in the distribution of T-NPA and T-NPB were observed.
482   However, if any, T-NPB appeared to move faster than T-NPA.
483   Figure 6 shows fluorescence microscopy images of ileum samples from the animals
484   treated with Lumogen® F Red-labelled nanoparticles. NP displayed a localisation mainly
485   restricted to the mucus layer protecting the epithelium both in the stomach (Figure 6A)
486   and in the ileum (Figures 6B and 6C). On the contrary, for nanoparticles containing
487   thiamine it was evident that these carriers were capable of reaching the epithelium and
488   interact broadly with the intestinal cells (Figures 6E, 6F, 6H and 6I).
489
490   **4. Discussion**
491   In this work, the effect of the preparative process of thiamine-coated nanoparticles on
492   their distribution within the gut (after oral administration) was evaluated. For this
493   purpose, two different procedures for the preparation of these nanocarriers were
494   compared.
495   In the former, a conventional bottom-up procedure with two consecutive steps was
496   employed (Salman et al., 2007). In this approach, the copolymer of methyl vinyl ether
497   and maleic anhydride (Gantrez® AN) was initially transformed into poly(anhydride)
498   nanoparticles and, subsequently, functionalized with thiamine before purification and
499   drying. With this approach, the resulting thiamine-coated nanoparticles (T-NPA)
500   displayed a mean size of about 215 nm and a negative zeta potential of –38 mV (Table
501   2). These physico-chemical characteristics were quite similar to that observed for bare
502   nanoparticles (NP); although T-NPA, when observed by SEM (Figure 2A), displayed a
503   rougher surface than NP. In addition, the amount of thiamine associated with T-NPA
504   nanoparticles was about 15 µg/mg with a surface density (dT) of about 0.98 molecules
505   per nm^2. In spite of its simplicity, this typical approach may be not the most adequate
506   when biologically active compounds of hydrophilic nature (e.g., therapeutic peptides
507   and proteins) have to be encapsulated into these nanoparticles. In fact, during the
508   functionalization process, a significant fraction of the encapsulated compound may be
509   lost due to a premature release in the medium in which the binding takes place (Dalwadi
510   et al., 2005; Patil et al., 2009; Tang et al., 2009). This migration of the loaded compound
511   (from the nanoparticle matrix through the external medium) may also affect the surface
512   properties of the resulting nanoparticles and, thus, their behaviour in vivo.
513   In the latter, the first step was to build a conjugate (between Gantrez® AN and thiamine)
514   to be used as material for the preparation of the functionalized nanoparticles.
515   Nanoparticles from GT were obtained by forming calcium ion bridges between
516   neighbouring carboxylic acid groups of the polymer backbone. The presence of calcium
517   was necessary to confer stability to the resulting nanoparticles. This strategy is more
518   time-demanding due to the necessary synthesis of the pre-cursor. However, the
519   subsequent preparation step to form the nanoparticles is simpler and shorter,
520   minimizing the negative effects on the payload.
521   In our case, the synthesized conjugate between Gantrez® AN and vitamin B1 contained
522   about 9 µg thiamine per mg, with a substitution degree of 13%. From this polymer
523   conjugate, the resulting nanoparticles (T-NPB) displayed a slightly higher mean size (227

524 vs 215 nm, Table 2) and a lower negative zeta potential (-30 vs -38 mV, Table 2) than T-
525 NPA. By SEM, T-NPB presented a similarly rough surface as did T-NPA (Figure 2B and 2C).
526 However the main concern by using the Gantrez® AN-thiamine conjugate was the
527 impossibility of precisely determined the number of thiamine molecules on the surface
528 of the resulting nanoparticles (T-NPB). For other types of hydrophilic conjugates, such
529 as copolymers between polyesters and poly(ethylene glycol) (e.g. PLGA-PEG), it has been
530 confirmed that during the formation of nanoparticles the polyester chains form the core,
531 while PEG chains are oriented to the water phase (Li et al., 2001; Schubert et al., 2011).
532 In our case, it is plausible to imagine that the hydrophilic residues of thiamine would be
533 mainly exposed on the surface of nanoparticles. In order to confirm this hypothesis, the
534 mucus penetrating properties of nanoparticles as well as their fate *in vivo* was studied.
535 When T-NPA or T-NPB were orally administered to rats, they distributed along the
536 gastrointestinal tract (Figure 4) with a lower tendency to concentrate in the stomach of
537 animals than bare nanoparticles. This observation was corroborated by the
538 measurement of the fluorescence marker associated with the nanoparticles in different
539 gut sections (Figure 5). Thus, 2 h post-administration, about 15% of the given dose of NP
540 was quantified in contact with the stomach mucosa. This value represented at least 3-
541 times greater dose than for T-NPA or T-NPB. On the contrary, the amounts of T-NPA or
542 T-NPB adhered to the small intestine mucosa (mainly in the distal jejunum and proximal
543 ileum, I2 segment in Figure 5A) were significantly higher than for NP (p<0.001). Four
544 hours post-administration, the amount of bare nanoparticles adhered to the gut mucosa
545 was very low, whereas, for T-NPA and T-NPB, the fraction of the given dose in close
546 contact with the small intestine mucosa remained higher than 30%. These observations
547 are in line with our previous results in which the coating of poly(anhydride)
548 nanoparticles with thiamine (T-NPA) increased 3-fold the capability of these
549 nanocarriers to develop adhesive interactions within the gut and, at the same time,
550 decreased their elimination rate from the mucosa (Salman et al., 2007). In addition, from
551 a microscopic point of view (Figure 6), it was clear that bare nanoparticles displayed a
552 different behaviour than thiamine-nanoparticles (T-NPA and T-NPB). Thus, within the
553 gut mucosa, NP was localized in the protective mucus layer confirming their
554 mucoadhesive capability (Arbós et al., 2002; Gamazo et al., 2015). On the contrary,
555 thiamine nanoparticles appeared to be capable of reaching the intestinal epithelium,
556 confirming their mucus permeating properties. These results agree well with those
557 obtained from the *in vitro* evaluation of the diffusion of the intestinal mucin by PGSE-
558 NMR (Figure 3, Table 3). Interestingly, the diffusion coefficient of intestinal mucin was
559 not affected when bare nanoparticles were added. However, when incubated with T-
560 NPA or T-NPB, there was a significant increase in the diffusion coefficient of the mucin
561 (about 5-fold). These differences can only be attributed to the presence of thiamine on
562 the surface of nanoparticles that would transform their surface, conferring slippery
563 properties and facilitating their permeability through a mucus gel layer. It is also worth
564 noting that the mucin alone, and due to its heterogeneous composition, fitted well to
565 two diffusion coefficients, as described previously (Pereira de Sousa et al., 2015a):
566 D_{fast}=8.3E-12 m^2/s, 21% of the signal, D_{slow}= 2.1 E-13 m^2/s, 79% of the signal.
567 On the other hand, when nanoparticles were added to the mucin samples the spectra
568 fitted best to 3 diffusion coefficients indicating that poly(anhydride) nanoparticles
569 possess a hydrophobic surface and one could imagine a strong interaction with the
570 hydrophobic portions of the mucin molecule, which would lead to a mucoadhesive

571 property and presumably a viscosification of the sample as the particles act as nodes for
572 the enhancement of the mucin gel cross-linking. However, the polymer backbone
573 forming the thiamine decorated nanoparticles has a highly dense coat of the low MW
574 and highly hydrophilic compound, thiamine, which one assumes will prevent an
575 interaction with the mucin network.
576
5. Conclusion
578 In summary, the mucoadhesive poly(anhydride) nanoparticles were transformed into
579 mucus-penetrating ones by their coating with vitamin B1. These thiamine-nanoparticles
580 displayed a high ability to diffuse and cross through the protective mucus layer in order
581 to reach the intestinal epithelium. Interestingly, thiamine-decorated nanoparticles may
582 be prepared by two different procedures. Both approaches yield nanocarriers with
583 similar physico-chemical and biodistribution properties. This result increases the
584 versatility of such nanocarriers as oral delivery systems for a number of biologically
585 active compounds.
586

593

References
595 Arbós, P., Arangoa, M.., Campanero, M.., Irache, J.., 2002. Quantification of the
596   bioadhesive properties of protein-coated PVM/MA nanoparticles. Int. J. Pharm.
597   242, 129–136. https://doi.org/10.1016/S0378-5173(02)00182-5
598 Areses, P., Agüeros, M.T., Quincoces, G., Collantes, M., Richter, J.Á., López-Sánchez,
599   L.M., Sánchez-Martínez, M., Irache, J.M., Peñuelas, I., 2011. Molecular Imaging
600   Techniques to Study the Biodistribution of Orally Administered 99mTc-Labelled
601   Naive and Ligand-Tagged Nanoparticles. Mol. Imaging Biol. 13, 1215–1223.
602   https://doi.org/10.1007/s11307-010-0456-0
603 Bourganis, V., Karamanidou, T., Samaridou, E., Karidi, K., Kammona, O., Kiparissides, C.,
604   2015. On the synthesis of mucus permeating nanocarriers. Eur. J. Pharm. Biopharm.
605   97, 239–249. https://doi.org/10.1016/J.EJPB.2015.01.021
606 Callaghan P.T., 1991. Principles of nuclear magnetic resonance microscopy, Oxford
607   Science Publications. Corby. https://doi.org/10.1118/1.596918
608 Dalwadi, G., Benson, H.A.E., Chen, Y., 2005. Comparison of diafiltration and tangential
609   flow filtration for purification of nanoparticle suspensions. Pharm. Res. 22, 2152–
610   2162. https://doi.org/10.1007/s11095-005-7781-2
611 des Rieux, A., Fievez, V., Garinot, M., Schneider, Y.-J., Préat, V., 2006. Nanoparticles as
612   potential oral delivery systems of proteins and vaccines: A mechanistic approach.
613   J. Control. Release 116, 1–27. https://doi.org/10.1016/J.JCONREL.2006.08.013
614 Ensign, L.M., Cone, R., Hanes, J., 2012. Oral drug delivery with polymeric nanoparticles:
615   The gastrointestinal mucus barriers. Adv. Drug Deliv. Rev. 64, 557–570.
616   https://doi.org/10.1016/J.ADDR.2011.12.009
617 Ferrari, A.C., Rodil, S.E., Robertson, J., Rodil, S.E., Robertson, J., 2003. Interpretation of

618 infrared and Raman spectra of amorphous carbon nitrides. Phys. Rev. B - Condens.
619 Matter Mater. Phys. 67, 1–20. https://doi.org/10.1103/PhysRevB.67.155306

620 Gamazo, C., Martín-Arbella, N., Brotons, A., Camacho, A.I., Irache, J.M., 2015. Mimicking
621 microbial strategies for the design of mucus-permeating nanoparticles for oral
622 immunization. Eur. J. Pharm. Biopharm. 96, 454–463.
623 https://doi.org/10.1016/J.EJPB.2015.01.010

624 Gómez, S., Gamazo, C., Roman, B.S., Ferrer, M., Sanz, M.L., Irache, J.M., 2007. Gantrez®
625 AN nanoparticles as an adjuvant for oral immunotherapy with allergens. Vaccine
626 25, 5263–5271. https://doi.org/10.1016/J.VACCINE.2007.05.020

627 Iglesias, T., López de Cerain, A., Irache, J., Martín-Arbella, N., Wilcox, M., Pearson, J.,
628 Azqueta, A., 2017. Evaluation of the cytotoxicity, genotoxicity and mucus
629 permeation capacity of several surface modified poly(anhydride) nanoparticles
630 designed for oral drug delivery. Int. J. Pharm. 517, 67–79.
631 https://doi.org/10.1016/J.IJPHARM.2016.11.059

632 Inchaurraga, L., Martín-Arbella, N., Zabaleta, V., Quincoces, G., Peñuelas, I., Irache, J.M.,
633 2015. In vivo study of the mucus-permeating properties of PEG-coated
634 nanoparticles following oral administration. Eur. J. Pharm. Biopharm. 97, 280–289.
635 https://doi.org/10.1016/J.EJPB.2014.12.021

636 Laffleur, F., Hintzen, F., Shahnaz, G., Rahmat, D., Leithner, K., Bernkop-Schnurch, A.,
637 2014. Development and in vitro evaluation of slippery nanoparticles for enhanced
638 diffusion through native mucus. Nanomedicine (Lond). 9, 387–396.
639 https://doi.org/10.2217/nnm.13.26

640 Li, Y.-P., Pei, Y.-Y., Zhang, X.-Y., Gu, Z.-H., Zhou, Z.-H., Yuan, W.-F., Zhou, J.-J., Zhu, J.-H.,
641 Gao, X.-J., 2001. PEGylated PLGA nanoparticles as protein carriers: synthesis,
642 preparation and biodistribution in rats. J. Control. Release 71, 203–211.
643 https://doi.org/10.1016/S0168-3659(01)00218-8

644 Netsomboon, K., Bernkop-Schnürch, A., 2016. Mucoadhesive vs. mucopenetrating
645 particulate drug delivery. Eur. J. Pharm. Biopharm. 98, 76–89.
646 https://doi.org/10.1016/J.EJPB.2015.11.003

647 Patil, Y.B., Toti, U.S., Khdair, A., Ma, L., Panyam, J., 2009. Single-step surface
648 functionalization of polymeric nanoparticles for targeted drug delivery.
649 Biomaterials 30, 859–866. https://doi.org/10.1016/J.BIOMATERIALS.2008.09.056

650 Pelaseyed, T., Bergstrom, J.H., Gustafsson, J.K., Ermund, A., Birchenough, G.M.H.,
651 Schutte, A., van der Post, S., Svensson, F., Rodriguez-Pineiro, A.M., Nystrom, E.E.L.,
652 Wising, C., Johansson, M.E. V, Hansson, G.C., 2014. The mucus and mucins of the
653 goblet cells and enterocytes provide the first defense line of the gastrointestinal
654 tract and interact with the immune system. Immunol. Rev. 260, 8–20.
655 https://doi.org/10.1111/imr.12182

656 Pereira de Sousa, I., Cattoz, B., Wilcox, M.D., Griffiths, P.C., Dalgliesh, R., Rogers, S.,
657 Bernkop-Schnürch, A., 2015a. Nanoparticles decorated with proteolytic enzymes,
658 a promising strategy to overcome the mucus barrier. Eur. J. Pharm. Biopharm. 97,
659 257–264. https://doi.org/10.1016/J.EJPB.2015.01.008

660 Pereira de Sousa, I., Steiner, C., Schmutzler, M., Wilcox, M.D., Veldhuis, G.J., Pearson,
661 J.P., Huck, C.W., Salvenmoser, W., Bernkop-Schnürch, A., 2015b. Mucus
662 permeating carriers: formulation and characterization of highly densely charged
663 nanoparticles. Eur. J. Pharm. Biopharm. 97, 273–279.
664 https://doi.org/10.1016/J.EJPB.2014.12.024

665 Roger, E., Lagarce, F., Garcion, E., Benoit, J.-P., 2010. Biopharmaceutical parameters to
666   consider in order to alter the fate of nanocarriers after oral delivery. Nanomedicine
667   (Lond). 5, 287–306. https://doi.org/10.2217/nnm.09.110

668 Salman, H.H., Gamazo, C., Agüeros, M., Irache, J.M., 2007. Bioadhesive capacity and
669   immunoadjuvant properties of thiamine-coated nanoparticles. Vaccine 25, 8123–
670   8132. https://doi.org/10.1016/j.vaccine.2007.09.044

671 Salman, H.H., Gamazo, C., Campanero, M.A., Irache, J.M., 2006. Bioadhesive
672   mannosylated nanoparticles for oral drug delivery. J. Nanosci. Nanotechnol. 6,
673   3203–3209.

674 Salman, H.H., Gamazo, C., Campanero, M.A., Irache, J.M., 2005. Salmonella-like
675   bioadhesive   nanoparticles.   J.   Control.   Release   106,   1–13.
676   https://doi.org/10.1016/J.JCONREL.2005.03.033

677 Schubert, S., Delaney, Jr, J.T., Schubert, U.S., 2011. Nanoprecipitation and
678   nanoformulation of polymers: from history to powerful possibilities beyond
679   poly(lactic acid). Soft Matter 7, 1581–1588. https://doi.org/10.1039/C0SM00862A

680 Schulz, J.D., Gauthier, M.A., Leroux, J.-C., 2015. Improving oral drug bioavailability with
681   polycations?   Eur.   J.   Pharm.   Biopharm.   97,   427–437.
682   https://doi.org/10.1016/J.EJPB.2015.04.025

683 Singh, R., Lillard, J.W., 2009. Nanoparticle-based targeted drug delivery. Exp. Mol.
684   Pathol. 86, 215–223. https://doi.org/10.1016/J.YEXMP.2008.12.004

685 Stilbs, P., Paulsen, K., Griffiths, P.C., 1996. Global Least-Squares Analysis of Large,
686   Correlated Spectral Data Sets: Application to Component-Resolved FT-PGSE NMR
687   Spectroscopy. J. Phys. Chem. 100, 8180–8189. https://doi.org/10.1021/JP9535607

688 Suk, J.S., Lai, S.K., Wang, Y.-Y., Ensign, L.M., Zeitlin, P.L., Boyle, M.P., Hanes, J., 2009. The
689   penetration of fresh undiluted sputum expectorated by cystic fibrosis patients by
690   non-adhesive   polymer   nanoparticles.   Biomaterials   30,   2591–2597.
691   https://doi.org/10.1016/J.BIOMATERIALS.2008.12.076

692 Tang, B.C., Dawson, M., Lai, S.K., Wang, Y.-Y., Suk, J.S., Yang, M., Zeitlin, P., Boyle, M.P.,
693   Fu, J., Hanes, J., 2009. Biodegradable polymer nanoparticles that rapidly penetrate
694   the human mucus barrier. Proc. Natl. Acad. Sci. U. S. A. 106, 19268–19273.
695   https://doi.org/10.1073/pnas.0905998106

696 Taylor, C., Allen, A., Dettmar, P.W., Pearson, J.P., 2004. Two rheologically different
697   gastric mucus secretions with different putative functions. Biochim. Biophys. Acta
698   - Gen. Subj. 1674, 131–138. https://doi.org/10.1016/J.BBAGEN.2004.06.007

699 Zabaleta, V., Ponchel, G., Salman, H., Agüeros, M., Vauthier, C., Irache, J.M., 2012. Oral
700   administration of paclitaxel with pegylated poly(anhydride) nanoparticles:
701   Permeability and pharmacokinetic study. Eur. J. Pharm. Biopharm. 81, 514–523.
702   https://doi.org/10.1016/J.EJPB.2012.04.001

703
704

Figure Captions

Figure 1. Confirmation of GT conjugate. (A) Schematic representation of the formation of the new conjugate. (B) IR spectra of Gantrez® AN polymer (G) and Gantrez® *AN-*thiamine conjugate (GT).

Figure 2. Scanning electron microphotographs of "naked" poly(anhydride) nanoparticles (A), T-NPA (B) and T-NPB (C). In the above right side, a magnification of a section of each microphotograph is shown.

Figure 3. PGSE-NMR spectra of mucin alone (A3) obtained from the two components forming the gel (A1-A2) and mucin in the presence of nanoparticles (B4) obtained from the three components forming the gel (B1-B3). x axis: frequency; y axis: intensity and z axis: trace.

Figure 4. Volume rendered fused SPECT-CT images from representative animals 2 h after administration of ^{99m}Tc-labelled NP by oral gavage. NP: "naked" nanoparticles; T-NPA: thiamine-coated poly(anhydride) nanoparticles; T-NPB: Gantrez® AN-thiamine nanoparticles.

Figure 5. Percentage of the given dose in close contact with the mucosa of the different parts of the gastrointestinal tract. (A) Two-hours and (B) 4-hours post-administration. NP: "naked" nanoparticles; T-NPA: thiamine-coated poly(anhydride) nanoparticles; T-NPB: Gantrez® AN-thiamine nanoparticles (n=3). STO : stomach ; I1, I2, I3 : small intestine portions ; CE : caecum.

Figure 6. Fluorescence microscopic visualisation of nanoparticles containing thiamine (T-NPA and T-NPB) and control ones (NP) in a longitudinal section of the stomach mucosa and ileum of rats 2 hours post administration. A: NP in the stomach mucosa; B and C: NP in the ileum mucosa; D: T-NPA in the stomach; E and F: T-NPA in the ileum mucosa; G: T-NPB in the stomach mucosa; H and I: T-NPB in the ileum mucosa.
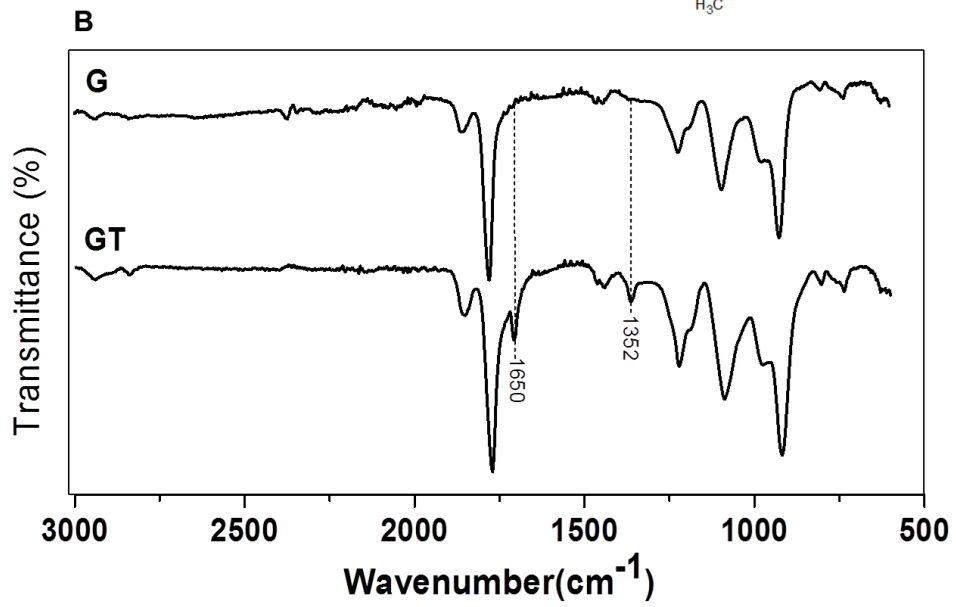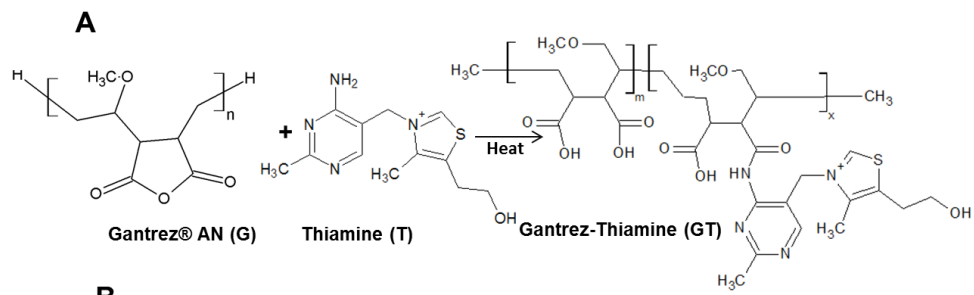
A

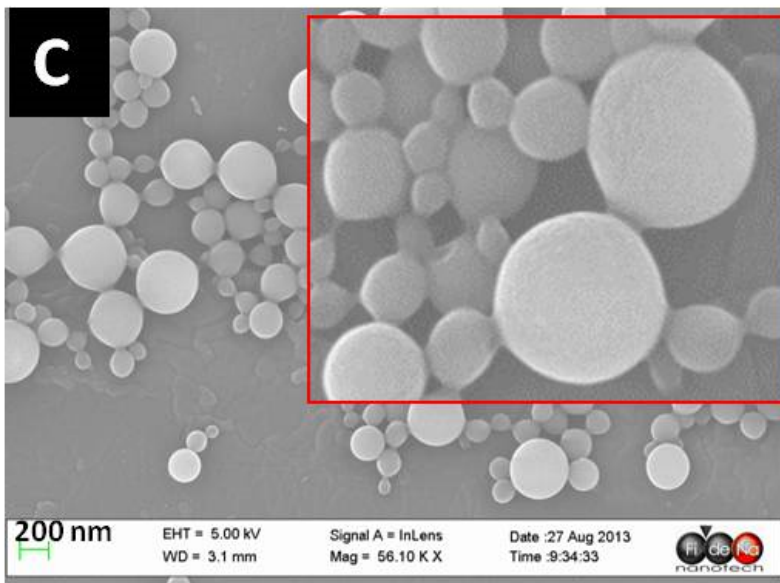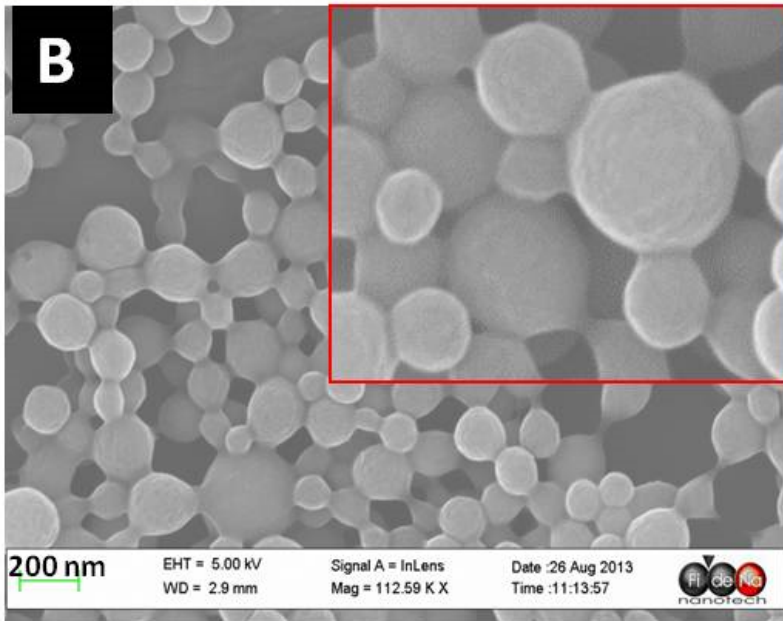Gantrez® AN (G)   Thiamine (T)   Gantrez-Thiamine (GT)

B

G

GT

1650

1352

Transmittance (%)
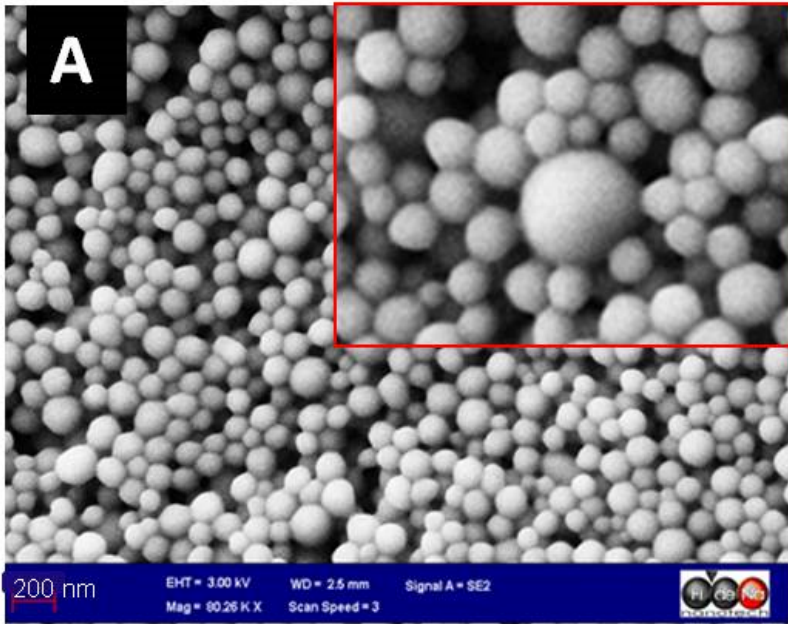
Wavenumber(cm^{-1})
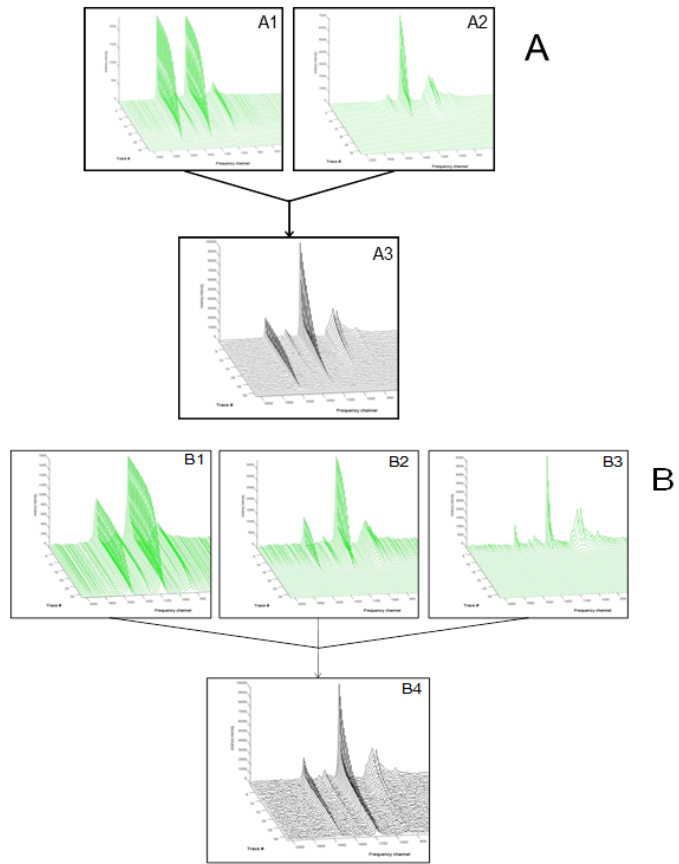
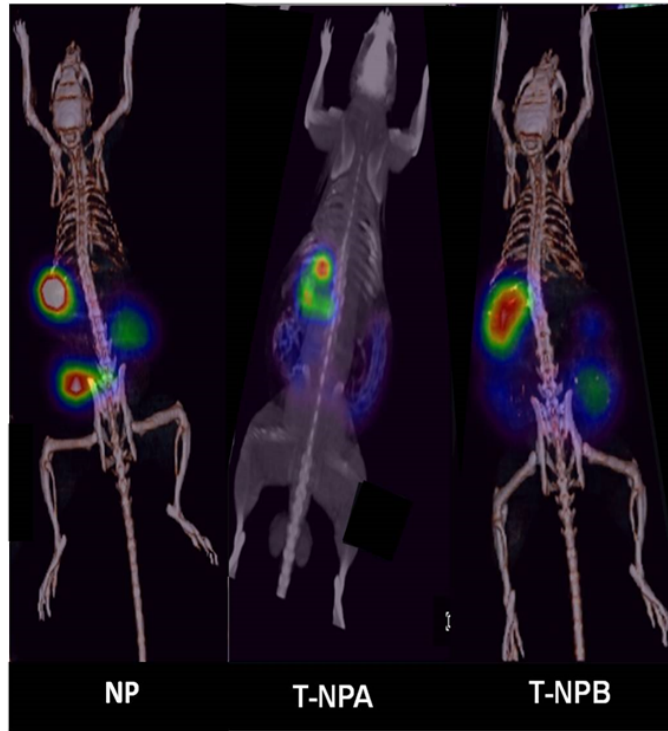3000   2500   2000   1500   1000   500

740
741
742

18

743

744
745

Fig 3

746
747
748

Fig 4

749
750
751
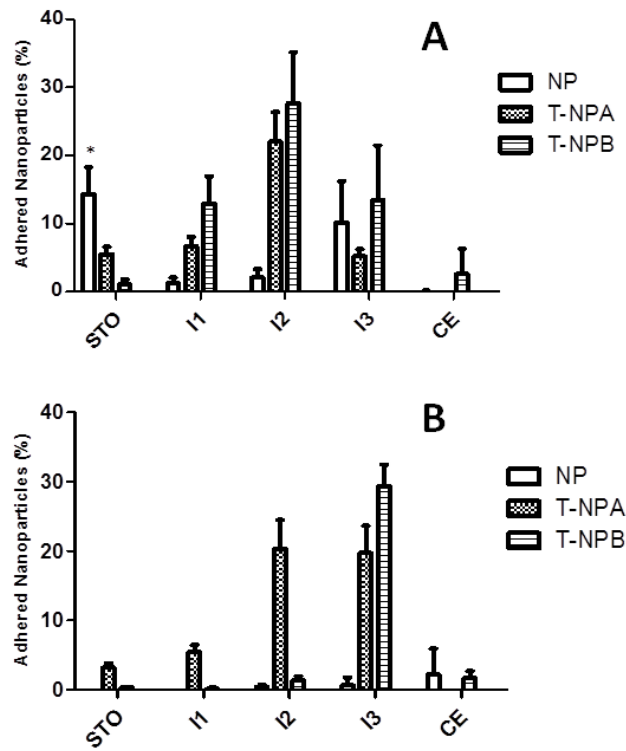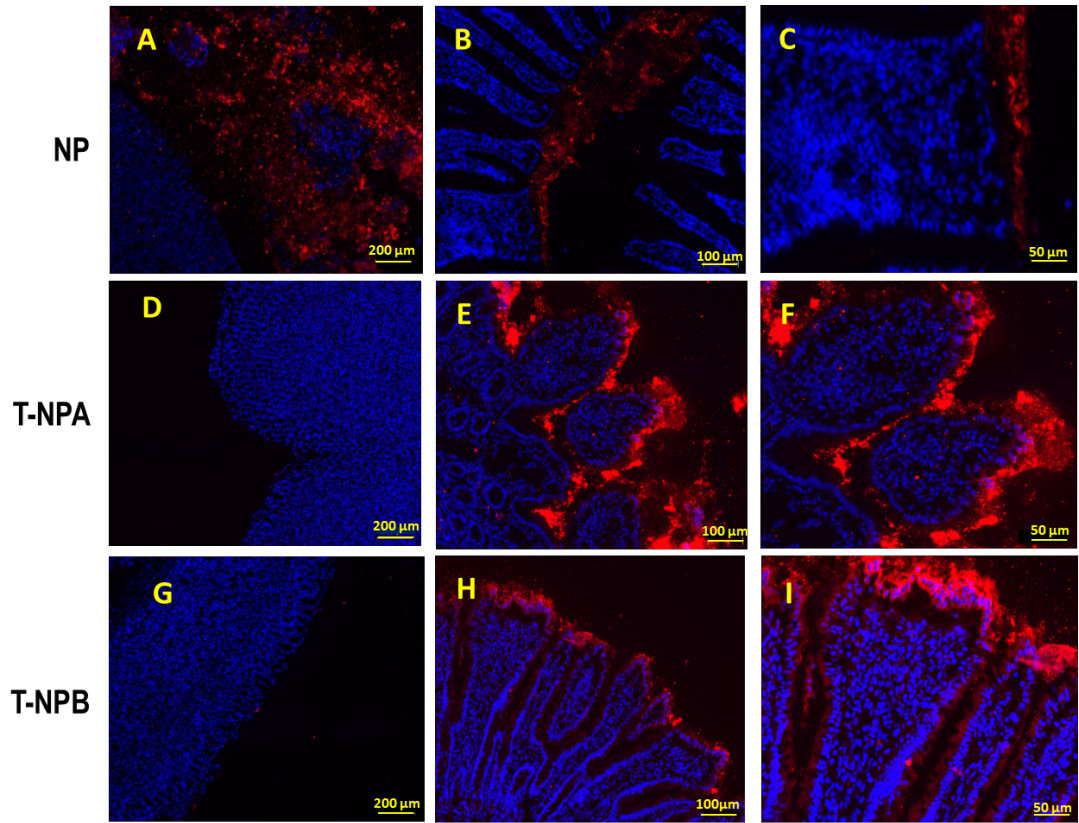
Fig 5

752
753
754

Table 1. Physico-chemical characterization of Gantrez® AN and its conjugate with thiamine (GT). For titration and HPLC experiments, data expressed as mean ± SD (n=3).

Polymer	C%	H%	O%	% Free -COOH	DS (%)	MW (kDa)	Thiamine content (µg/mg G)
G	53.49	5.18	41.33	100 ± 0	0	95.50	-
GT	53.19	5.58	41.23	87 ± 1	13	96.33	8.7 ± 0.6

Table 2. Physico-chemical characterization of nanoparticles. NP: "naked" poly(anhydride) nanoparticles; T-NPA: poly(anhydride) nanoparticles coated with thiamine; T-NPB: Gantrez® *AN*-thiamine conjugate nanoparticles. Data expressed as mean ± SD (n=3).

Formulation	Size (nm)	PDI	Zeta Potential (mV)	Thiamine (µg/mg NP)
NP	213 ± 4	0.031 ± 0.012	-36.2 ± 3.0	-
T-NPA	215 ± 3	0.128 ± 0.023	-38.5 ± 3.2	15 ± 0.6
T-NPB	227 ± 5	0.092 ± 0.020	-30.6 ± 5.4	ND

Table 3. Diffusion coefficients of the mucin in the presence of nanoparticles. The experiments were carried out with intestinal mucin. D1-D3: diffusion coefficients of the components forming the mucin. D: diffusion coefficient; R: Ratio between the diffusion coefficients obtained for the nanoparticle formulation and mucin. Intensities of the diffusion coefficients of each component in brackets.

Formulation	D1 ($/10^{11}\,m^2\,s^{-1}$)	D2 ($/10^{11}\,m^2\,s^{-1}$)	D3 ($/10^{11}\,m^2\,s^{-1}$)	$D_{weighted}$ ($/10^{11}\,m^2\,s^{-1}$)	R
Mucin	-	0.021 (21%)	0.830 (79%)	0.66	1.0
NP	0.002 (21%)	0.051 (16%)	1.200 (63%)	0.79	1.2
T-NPA	0.002 (11%)	0.249 (18%)	4.591 (71%)	3.29	5.0
T-NPB	0.004 (14%)	0.391 (22%)	4.780 (64%)	3.12	4.7